

RESEARCH ARTICLE

Design and Evaluation of a Spherical Multi-Layered Unit for String Jamming Mechanisms

RYOHEI MICHIKAWA¹ AND FUMITOSHI MATSUNO², (Senior Member, IEEE)¹Department of Mechanical Engineering and Science, Kyoto University, Kyoto 606-8501, Japan²Faculty of Engineering, Osaka Institute of Technology, Osaka 535-8585, Japan

Corresponding author: Fumitoshi Matsuno (fumitoshi.matsuno@oit.ac.jp)

ABSTRACT In soft robotics, it is desirable to be able to switch between two states, namely a soft state for adaptation to the environment and a rigid state for the transmission of forces. String jamming mechanisms, composed of bead-like connected units, have gained attention for their ability to switch between these states. This paper presents the design and evaluation of a new multi-layered unit for string jamming mechanisms aimed at enhancing holding torque while maintaining high flexibility. The proposed spherical-layered unit addresses the dual-state challenge by introducing a spherical multi-layer structure that enhances frictional forces and improves holding torque in the rigid state without compromising flexibility in the soft state. Through theoretical analysis and experimental validation, we demonstrate that the proposed unit achieves an improvement in each fitting performance and holding torque compared to existing designs. This study provides guidelines for future applications of variable stiffness technologies, particularly in soft robotics, manipulators, and haptic devices.

INDEX TERMS Flexible structures, jamming, physical design, rigidity, soft robotics.

I. INTRODUCTION

Soft robotics offer numerous potential applications due to their ability to absorb shocks and conform to an object's shape. One such soft robotics technology utilizes the jamming transition phenomenon in powders, beads, and paper [1], [2], [3]. Known as jamming, this technique generates a stiff state from a soft state through the compression of a many-body system. Unlike general soft robotics, this technology has drawn attention for its ability to switch between soft and stiff states. Typically, conventional jamming systems use chambers filled with materials like coffee powder or paper bundles. When a vacuum is applied, the contents are compressed, triggering the jamming transition. This approach, referred to as granular or layer jamming based on the material used, has been applied in grippers [4], [5], soft actuators [6], [7], and haptic devices [8], acting as a

variable-stiffness material. However, issues such as the fragility of the chamber structure [9], [10] and the limitations of stiffness due to atmospheric pressure [11], [12] remain significant challenges.

Another jamming technology, known as the string jamming mechanism, has garnered attention [9], [10], [11], [12], [13], [14], [15], [16]. This mechanism consists of solid components with spherical or cylindrical contact surfaces connected by internal wires, allowing transitions between a flexible, string-like state and a rigid, fixed shape (Fig. 1, see [9]). The switching is achieved by applying tension to the internal wires, generating static friction at the joints to lock the angles. Compared to granular or layer jamming, string jamming is more durable due to its solid parts, and its maximum stiffness is determined by wire tension, providing adjustable rigidity. As a result of these characteristics, string jamming mechanisms have been utilized in fire-resistant grippers [13] made with metal components, as well as in lightweight haptic devices [14] requiring only one

The associate editor coordinating the review of this manuscript and approving it for publication was Tommaso Lisini Baldi¹.

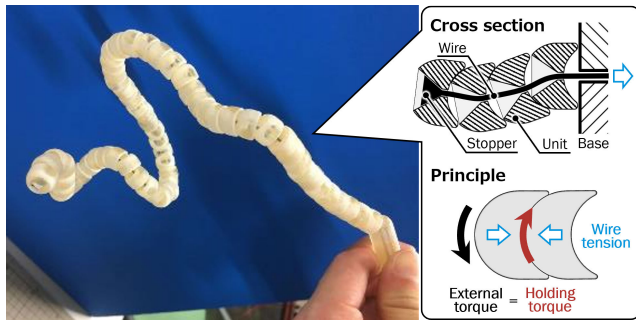


FIGURE 1. Overview of the string jamming mechanism. A wire connects rigid parts with uneven structures on the front and back [9]. The shape is fixed by pulling the inner wire.

actuator. Furthermore, applications such as exploring or operating in confined spaces like pipes or animal burrows are anticipated, taking advantage of its string-like flexibility [10], [17].

A jamming unit (or simply unit) is a repeated pattern describing the characteristics of the string jamming mechanism [9]. Various unit shapes have been proposed in previous studies [10], [11], [12], [13], [14], [15], [16], but the researches focused on improving the jamming mechanism's ability to hold its shape in the rigid state (referred to as holding torque) were conducted by Mukaide et al. [10] and Michikawa et al. [14]. They introduced a cylindrical multilayer unit shape, which reportedly improved holding torque. However, there are problems such as decreased fitting performance due to the reduction in degrees of freedom (DoFs) from three to one.

Our previous study introduced a new unit shape with a spherical multilayer structure while maintaining three DoFs [15]. However, there are issues such as a low improvement ratio in holding torque and increased distance between units. Additionally, there was a lack of quantitative comparison of fitting performance and insufficient analysis of holding torque changes with varying layer numbers. In this study, we redesigned the spherical-layer-type to improve its characteristics while adhering to the unit shape's design guidelines [15]. We also evaluated fitting performance using the maximum curvature value. Finally, we measured and compared holding torque across different unit shapes and layer numbers. Through these analyses, we clarify the strengths and weaknesses of the spherical-layer-type unit and provide guidelines for future applications.

II. EXISTING STRING JAMMING UNITS

A string jamming mechanism consists of solid, bead-shaped components linked together. Tension applied to a wire threaded through the center generates friction between the parts, thereby locking each joint angle and fixing the shape of the entire mechanism. In its rigid state, the ability of the mechanism to keep its shape is characterized by the maximum external torque at which the joint angles remain unchanged, referred to as the holding torque. The holding torque is typically proportional to the wire tension [10], [14], [15].

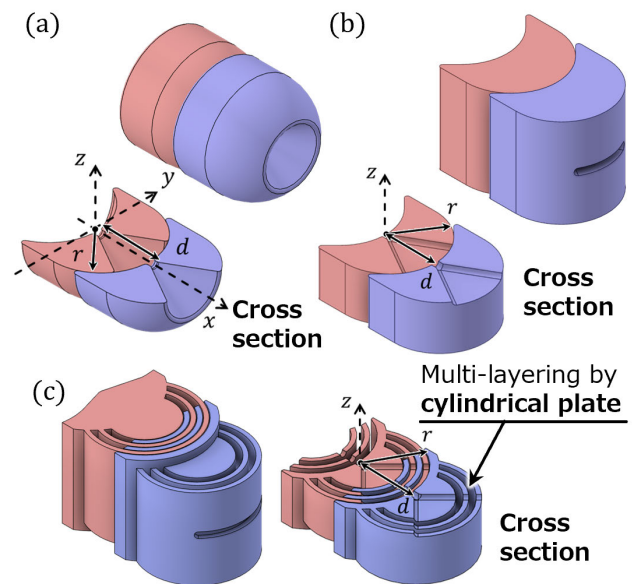


FIGURE 2. Shapes of existing jamming units [9], [10], r : unit radius, d : separation of axes. (a) 3d-bead-type unit. (b) 1d-bead-type unit. (c) radial-layer-type unit with two layers.

A higher holding torque for a given wire tension indicates a more efficient jamming mechanism.

Figure 2 shows three existing types of jamming units proposed by Fujimoto, Mukaide, et al. [9], [10]. The 3d-bead-type unit in Fig. 2 (a) is the simplest unit [9]. The bowl-shaped concavo-convex structure at the front and back of the 3d-bead-type unit prevents the overall shape from changing under wire tension. This design prevents the joint from unintentionally straightening under wire tension. The 3d-bead-type unit has a corn-shaped hole that allows the wire to pass through the center of the unit. Due to its small size and simple shape, the unit can accommodate more joints per unit length, resulting in high fitting performance. However, it is limited as a variable-stiffness mechanism because of its low holding torque.

Mukaide et al. developed the 1d-bead-type unit in Fig. 2 (b), featuring a cylindrical contact surface and a reduction in DoF from three to one. The 1d-bead-type unit uses a fan-shaped wire hole instead of the conical shape in the 3d-bead-type. The conical hole allows only a small motion range (about 30°) due to the significant reduction in contact area with increased motion range, as shown in Fig. 2 (a). Conversely, the fan-shaped wire hole allows for a larger motion range (about 45°) without significantly reducing the contact area, as shown in Fig. 2 (b). A key feature of the 1d-bead-type unit is its increased motion range. However, despite the increased motion range, the DoF is reduced from three to one, lowering fitting performance compared. Moreover, the 1d-bead-type unit was introduced as a reference design for the development of the radial-layer-type unit, discussed below, and its holding torque remains low.

To solve the issue of low holding torque, Mukaide et al. also developed the radial-layer-type unit, which is an

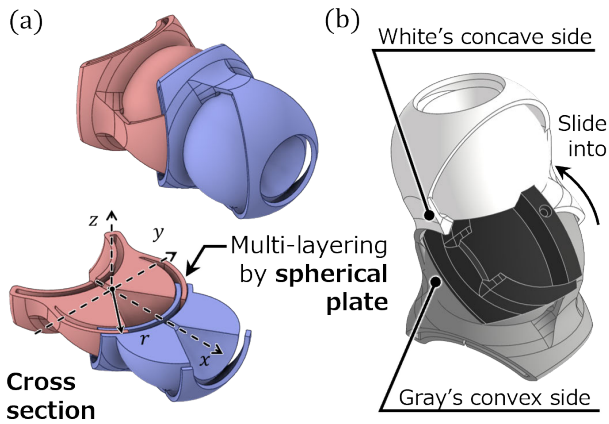


FIGURE 3. Proposed spherical-layer-type units. (a) Appearance of two connected units. (b) Connection of the two units. The white and black parts are joined once the white and gray parts are connected.

enhanced version of the 1d-bead-type unit, as shown in Fig. 2 (c). The holding torque of these units is enhanced by their multilayered cylindrical structure, where each pair of units features multiple friction surfaces. While the motion range is increased for the same reason as the 1d-bead-type unit, a key limitation is that each joint has only one DoF, resulting in lower fitting performance in three-dimensional space. Mukaide et al. prototyped and verified a unit with two layers, but did not compare the effect of the number of layers. A similar study by Michikawa et al. [14] also handled the radial-layer-type unit. The study reveals the influence of some shape features on the holding torque, but only considered a one layer configuration. The other unit proposed by Mukaide et al. is the comb-layer-type unit, which has a different multilayer structure. However, because it cannot form a string jamming mechanism that can adapt to three-dimensional space, we do not consider it as a comparison target in this study.

The existing units are summarized as 3d-bead-type units with high fitting performance and low holding torque, 1d-bead-type unit with low fitting performance and low holding torque, and radial-layer-type unit with low fitting performance and high holding torque. We have proposed the spherical-layer-type unit in [15] combines the short inter-axis distance and three DoFs of the 3d-bead-type unit with the multilayer structure of the radial-layer-type unit, and thus has improved holding torque while maintaining high fitting performance.

III. SPHERICAL-LAYER-TYPE JAMMING UNIT

This section describes the design of the spherical-layer-type unit. The key feature of this unit is its spherical multilayer structure, allowing units to connect in a chain. Other multilayer structure proposed by Mukaide et al. [10] consists of cylinders with different diameters or alternating combs, enabling connection through translational movement. However, the spherical shell structure required for three DoF motion cannot be normally connected. Thus, the primary

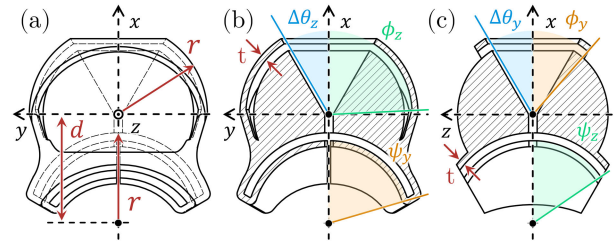


FIGURE 4. Design parameters of the spherical-layer-type unit. r : radius of the unit, d : distance between axes, t : thickness of the spherical plates, $\Delta\theta_{y,z}$: motion ranges around the y and z axes, $\phi_{y,z}$: angle widths on the convex side around the y and z axes, $\psi_{y,z}$: angle widths on the concave side around the y and z axes. (a) Overview, (b) cross section of the x - y plane, (c) cross section of the x - z plane.

challenge in developing the spherical-layer-type unit is designing a structure that maintains the spherical multilayer configuration while allowing connection. As explained in the next section, the basic concept of a solution to this problem was proposed in our previous research [15]. Nevertheless, issues such as low improvement ratio in holding torque and the longer distance between joint axes compared to the radial-layer-type unit remained. Therefore, we revisited the design in this study, while adhering to the basic principles of the existing spherical-layer-type unit.

A. BASIC DESIGN CONCEPT [15]

Figure 3 (a) shows the designed spherical-layer-type unit's appearance and cross-section. The unit is fabricated in two parts [Fig. 3 (b), black and white], which are joined after connecting units to realize a spherical shell structure capable of assembly. As shown in Fig. 3, the connection procedure is as follows: i) Slide the concave spherical plate of the white part of the upper unit into the convex spherical plate of the lower gray unit. ii) Slide the black spherical plate of the upper unit into the convex spherical plate of the lower gray unit. iii) Join and bond the white and black parts to complete the upper unit. Detailed motion can be seen in the supplementary video. Another method to realize the spherical shell structure is fully integrated molding using a 3D printer based on powder sintering. However, this method was not adopted because it makes it impossible to change the number of units or replace damaged ones. For simplicity, the one-layer unit in Fig. 3 is used in the following explanations, but two- or three-layer units are also possible. Increasing the number of layers should enhance the holding torque, but it also limits the reduction of the unit's size.

B. DESIGN OF GEOMETRIC PARAMETERS

Figure 4 illustrates that each unit has one convex plate and one concave plate. The unit's radius is r , and the distance between joint axes is d [Fig. 4 (a)]. The convex plate and the ball part feature conical holes to allow wire movement. The wire bends at the center of the ball part, aligning with the joint center, so the path length remains constant regardless of joint angle. While r is freely determined as the representative unit length,

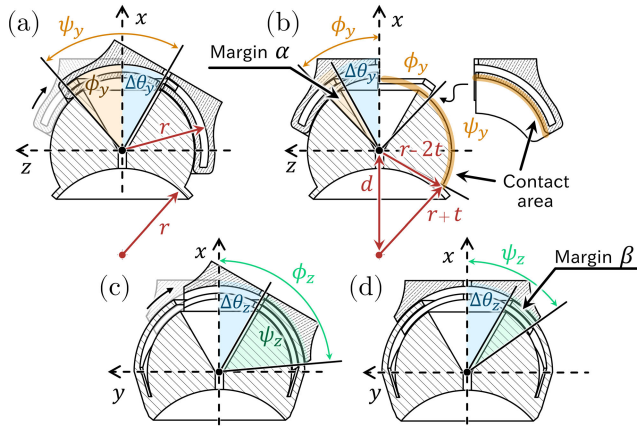


FIGURE 5. Cross sections of the x - z plane are shown in (a) and (b). Cross sections of the x - y plane are shown in (c) and (d). (a) Geometric constraint when a joint bends a maximum around the y axis. (b) Relationship between the margin α and other parameters, and, geometric constraint on the distance d . (c) Geometric constraint when a joint bends a maximum around the z axis. (d) Relationship between the margin β and other parameters.

d depends on the spherical shell plate parameters described below.

The spherical shell plate has seven parameters as shown in Fig. 4 (b) and (c). t : plate thickness, including the clearance. $\Delta\theta_{y,z}$: wire motion range around the y and z axes (joint motion angles). $\phi_{y,z}$: arc angles of convex plate on the cross-section perpendicular to the y and z axes. $\psi_{y,z}$: arc angles of concave plate on the cross-section perpendicular to the y and z axes. Among these, t and $\Delta\theta_{y,z}$ are freely adjustable design parameters, while $\phi_{y,z}$ and $\psi_{y,z}$ are constrained as described below. Note that the subscripts are reversed in Fig. 4 (b) and (c) due to the 90° displacement between the convex and concave plates.

First, the parameters ϕ_y and ψ_y with respect to rotation around the y axis are discussed. For the wire motion range $\Delta\theta_y$, convex plate's arc angle ϕ_y , and concave plate's arc angle ψ_y , from the geometric constraint in Fig. 5 (a), we derive:

$$\psi_y = \phi_y + \Delta\theta_y. \quad (1)$$

Since the convex plate has a hole for wire motion, the relation $\Delta\theta_y < \phi_y$ holds. By introducing a margin $\alpha > 0$, as shown in Fig. 5 (b), ϕ_y is given by:

$$\phi_y = \Delta\theta_y + \alpha. \quad (2)$$

To determine the geometric constraint on d , consideration of the assembly of the concave and convex sides of the spherical plates on the x - z cross section is required. When connecting two units, the concave plate of one unit must contact the central ball part of another unit before sliding into it, as shown in Fig. 5 (b). For the concave plate to make contact with the central ball part, the exposed portion of the ball part must be wider than the concave plate's arc angle ψ_y . Consequently, the polar angle of the ball part, measured from the x axis, is determined as $\phi_y + \psi_y$. Therefore, using the law of cosines, the distance d between the joints is given by the



FIGURE 6. Prototype of the spherical-layer-type unit with a single layer. The prototype is fixed in a rod-like shape, lifting a 300 g weight.

following equation:

$$(r + t)^2 = (r - 2t)^2 + d^2 - 2d(r - 2t) \cos(\pi - (\phi_y + \psi_y)). \quad (3)$$

Here, $r - 2t$ is the radius of the ball part, as it is the unit radius minus the thickness of two plates, and $r + t$ is the distance between the bottom edge of the ball part and the joint on the concave side. Using (1) and (2), (3) can be solved for d as follows:

$$d = -(r - 2t) \cos(3\Delta\theta_y + 2\alpha) + \sqrt{(r - 2t)^2 \cos^2(3\Delta\theta_y + 2\alpha) - 3t(t - 2r)}. \quad (4)$$

To enhance fitting performance, the inter-axial distance d needs to be minimized. Given that r , t , and $\Delta\theta_y$ are fixed values, from (4), d is determined solely by the margin α . The distance d increases monotonically with α , provided that $3\Delta\theta_y + 2\alpha = \phi_y + \psi_y \in (0, \pi]$. Thus, to achieve a smaller d , the margin α should be reduced. However, since the margin α represents the width of the narrowest part of the contact surface between the spherical plates, qualitatively, a larger α is required to generate higher friction and enhance the plate's strength. Although this trade-off could be formulated as an optimization problem, we avoided such an approach because mathematical models for frictional force and plate strength are currently unavailable. Consequently, we addressed the problem through a trial-and-error process, using FEM to check the strength and fabricating a prototype for validation.

Finally, the parameters ϕ_z and ψ_z with respect to rotation around the z axis are discussed. For the wire motion range $\Delta\theta_z$, the convex plate's arc angle ϕ_z , and the concave plate's arc angle ψ_z , the following relationship holds according to the geometric constraints in Fig. 5 (c):

$$\phi_z = \psi_z + \Delta\theta_z. \quad (5)$$

Similar to the y axis, we introduce a margin $\beta > 0$ as shown in Fig. 5 (d), leading to:

$$\psi_z = \Delta\theta_z + \beta. \quad (6)$$

Since $\Delta\theta_z$ is a fixed constant, from (5) and (6), both ψ_z and ϕ_z are determined by the margin β . As ϕ_z increases, the arc angle



FIGURE 7. Measurement of the motion range of the spherical-layer type unit. Left: y, z axes, right: x axis.

of the convex plate on the x - y cross section also increases. Since the margin β represents the contact surface between the spherical plates, a larger margin enhances friction. The maximum value for β is set to $\beta = \pi - 2\Delta\theta_z$, ensuring that $\phi_z = 2\Delta\theta_z + \beta < \pi$ holds.

C. FABRICATED PROTOTYPE

The design parameters of the fabricated prototype are described. The unit radius $r = 13.5$ mm and the thickness of the spherical plate $t = 1.1$ mm. Here, the thickness of the plate is set to minimum value that can be fabricated remaining the strength [10]. The range of motion around the y and z axes is set at $\Delta\theta_y = \Delta\theta_z = 30^\circ$ to obtain a sufficient motion range relative to the motion range of the 3d-bead-type unit (30°). Considering the trade-off, the margin around the y axis is set at $\alpha \simeq 15^\circ$ by trial and error to maintain the friction and plate strength. As mentioned above, the margin around the z axis is set at $\beta = \pi - 2\Delta\theta_z = 30^\circ$.

Figure 6 shows the fabricated prototype of the spherical-layer-type unit. The units of the prototype are fabricated using a 3D printer (Form 3, Formlabs) with Tough 2000 resin. Because friction is significantly affected by surface quality, the stacking direction was unified, and sufficient cleaning and secondary curing were performed. The parts that made by separated were bonded using light-curing resin of the same material.

We measured the motion range of the fabricated prototype. The test part used for the measurement is a beam with both ends extended from one set of jamming units, which will be used in Section V. The measurement is shown in Fig. 7. The motion ranges $\Delta\theta_y$ and $\Delta\theta_z$ were confirmed to be equal to the design values of 30° . Although the motion range $\Delta\theta_x$ around the x axis is not a parameter that can be freely designed, the measured value was confirmed to be approximately 30° .

Furthermore, for the above parameters, we obtain $\phi_y = 45^\circ$, $\psi_y = 75^\circ$, $\phi_z = 90^\circ$, and $\psi_z = 60^\circ$ using (1), (2), (5), and (6). For the inter-axial distance d , we substitute the above parameters into (4) and obtain $d \simeq 16.7$ mm, resulting in $d/r \simeq 1.2$. This result is equivalent to that of the radial-layer-type unit [10] and shows an improvement over the previous spherical-layer-type unit [15]. Table 1 compares the number of DoFs, inter-axial distance, motion range, and multilayeredness between existing units and the our unit. The shown parameters of the existing types are based on [10], and they are improved parameters that we actually manufactured.

TABLE 1. Geometrical parameters of string jamming units.

Unit type	DoF	d/r	$\Delta\theta_{x,y,z}$	multi-layered
3D-Bead	3	1.1	$\infty, 30^\circ, 30^\circ$	
1D-Bead	1	1.1	$0^\circ, 0^\circ, 45^\circ$	
Radial-layer	1	1.2	$0^\circ, 0^\circ, 45^\circ$	✓
Spherical-layer	3	1.2	$30^\circ, 30^\circ, 30^\circ$	✓

d : inter-axial distance, r : unit radius,

$\Delta\theta_{x,y,z}$: motion range of a joint around each axis.

A mark ✓ indicates that the unit has a multilayered structure.

IV. COMPARISON OF FITTING PERFORMANCE

One of the characteristics of the string jamming mechanism is its fitting performance to the environment or objects. The fitting performance, which indicates how well the bead-like mechanism can conform to a “three-dimensional arbitrary shape,” generally improves as the number of DoFs of the joints increases, the distance d between joint axes decreases, and the motion range $\Delta\theta_{x,y,z}$ of each joint expands. However, it is difficult to fairly evaluate the fitting performance by directly comparing each element due to trade-offs among different unit types. We evaluate the fitting performance based on the maximum curvature κ^{\max} of the continuous curve that the discrete jamming mechanism can approximate [16]. By adopting the curvature κ^{\max} as an index, it is possible to determine the complexity of the shape (curve or surface) that can be approximated by the mechanism. This is important when constructing applications using jamming mechanisms. We also compare the approximation precision when each mechanism is approximated to a minimum curvature circle.

A. MAXIMUM CURVATURE

Since any arbitrary spatial curve can be approximated as a series of infinitesimal circular arcs, it is sufficient to consider only circular arcs. Thus, as the curve, we consider the circle of minimum radius $1/\kappa^{\max}$ that can contact three points on the jamming mechanism, which is modeled as a linkage [Fig. 8]. In other words, we consider the situation where the jamming mechanism contacts from the outside the minimum curvature circle at a certain point on a spatial curve. It is possible to evaluate the fitting performance independently of the number of units, as only local curve approximation is considered.

The units with three DoFs (3d-bead- and spherical-layer-type) are modeled as ball joints and are serially connected to compose a linkage model of the jamming mechanisms (called the “three-DoFs linkage model”) [Fig. 8 left]. In contrast, the units with one DoF (1d-bead- and radial-layer-type) are modeled as revolute joints, alternately connected as pitch and yaw joints to compose the linkage model of the jamming mechanisms (called the “one-DoF linkage model”) [Fig. 8 right]. This joint configuration is commonly employed in snake robots composed of one-DoF modular units to form a three-dimensional curve [18]. As shown in Table 1, the dimensionless quantity d/r is used as the link length, and $\Delta\theta_{x,y,z}$ is used as the motion range of the joint.

In the three-DoFs linkage model, the ball joint’s bending motion ranges ($\Delta\theta_y, \Delta\theta_z$) are equal, and thus we introduce

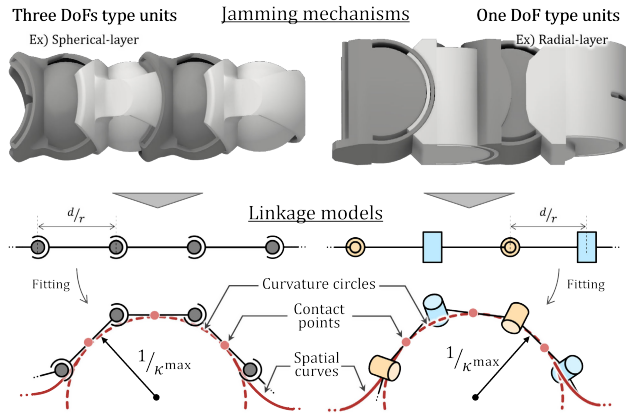


FIGURE 8. Modeling of the jamming mechanism as a linkage and the approximation of the maximum curvature of a spatial curve. Left: The three DoFs type units (3d-bead- and spherical-layer-type). Right: The one DoF type units (1d-bead- and radial-layer-type).

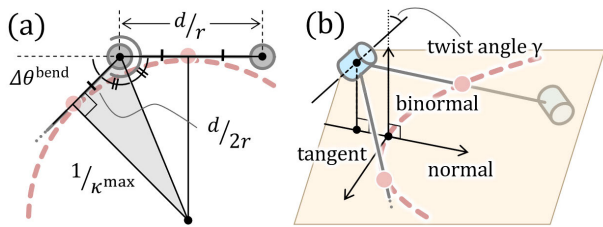


FIGURE 9. (a) Geometrical relation between the three-DoFs linkage model and the curvature circle. (b) Twist angle γ between the one-DoF linkage model and the approximated curve.

a new parameter $\Delta\theta^{\text{bend}} =: \Delta\theta_y = \Delta\theta_z$. The radius of the circle that contacts the linkage is minimized when all joints and the circle are in the same plane and all joints are bent to the motion limit $\Delta\theta^{\text{bend}}$. As shown in Fig. 9 (a), the minimum radius $1/\kappa^{\text{max}}$ is determined using the link length d/r and $\Delta\theta^{\text{bend}}$ as follows.

$$\frac{1}{\kappa^{\text{max}}} = \frac{d}{2r} \tan\left(\frac{\pi}{2} - \frac{\Delta\theta^{\text{bend}}}{2}\right). \quad (7)$$

Substituting $\Delta\theta^{\text{bend}} = 30^\circ$ and $d/r = 1.1$ for the 3d-bead-type unit, the maximum curvature is 0.487. Similarly, substituting $\Delta\theta^{\text{bend}} = 30^\circ$ and $d/r = 1.2$ for the spherical-layer-type unit, the maximum curvature is 0.447.

Unlike the three-DoFs linkage model, the one-DoF linkage model is not rotationally symmetric about the link longitudinal axis. Therefore, it is necessary to consider the twist angle γ between the reference joint's rotation axis and the binormal vector of the curve at the nearest point to the axis [Fig. 9 (b)]. The twist angle γ is determined by the torsion distribution of the entire spatial curve to be fitted. Since the approximated curvature circle is a part of an arbitrary spatial curve, γ must be treated as a variable that varies continuously. We show the maximum curvature κ^{max} as a function of the twist angle γ in Fig. 10 left. As seen from the figure, the optimal case where the maximum curvature is extremely large occurs when $\gamma \simeq 47.3^\circ$, and the worst cases occur when $\gamma = 90^\circ$ and 0° . The maximum curvature ranges are $\kappa^{\text{max}} \in [0.377, 0.533]$ for the

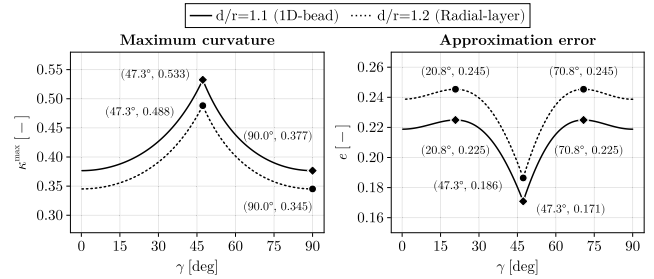


FIGURE 10. Relationship between the twist angle γ and each value in the one-DoF linkage model. Top: Maximum curvature κ^{max} . Bottom: Approximation error e .

1d-bead-type unit and $\kappa^{\text{max}} \in [0.345, 0.488]$ for the radial-layer-type unit. Because the twist angle γ can take any value, we use the average obtained by the following equation as a representative value:

$$\bar{\kappa}^{\text{max}} = \frac{\int_0^{\pi/2} \kappa^{\text{max}} d\gamma}{\int_0^{\pi/2} d\gamma}. \quad (8)$$

The average maximum curvature $\bar{\kappa}^{\text{max}}$ indicates the maximum curvature that can be approximated on average for any twist angle between the curve and the linkage. For the 1d-bead-type unit, $\bar{\kappa}^{\text{max}} = 0.421$, and for the radial-layer-type unit, $\bar{\kappa}^{\text{max}} = 0.386$.

B. APPROXIMATION ERROR

In addition to the maximum curvature, we also consider the error in approximating the minimum curvature circle. Even if the curvature is large (i.e., the mechanism can approximate fine shapes), the mechanism loses practical value if the approximation result deviates significantly from a smooth curve. Therefore, we define the approximation error between the minimum curvature circle to be approximated and the linkage model using the Hausdorff distance [19] as follows:

$$e =: \max \left\{ \max_{p \in \mathcal{C}} \min_{q \in \mathcal{L}} \|p - q\|, \max_{q \in \mathcal{L}} \min_{p \in \mathcal{C}} \|p - q\| \right\}. \quad (9)$$

Here, \mathcal{C} is the set of points on the minimum curvature circle, and \mathcal{L} is the set of points on the linkage model. In this situation, where the linkage model externally contacts the minimum curvature circle, the approximation error e is the perpendicular distance from each joint to the circular arc. This approximation error e is an index that indicates how smoothly the string jamming mechanism follows the curve.

For the three-DoFs linkage model, the approximation error e defined in (9) is the distance between the joint of the linkage and the nearest point on the minimum curvature circle. Thus, knowing the maximum curvature, the error e can be directly calculated as follows:

$$e = \sqrt{\left(\frac{d}{2r}\right)^2 + \left(\frac{1}{\kappa^{\text{max}}}\right)^2} - \frac{1}{\kappa^{\text{max}}} \quad (10)$$

Substituting $d/r = 1.1$ and $\kappa^{\text{max}} = 0.487$ for the 3d-bead-type unit, the approximation error is 0.072. Similarly, substituting

TABLE 2. Maximum curvature and approximation error.

Unit type	κ^{\max} or $\bar{\kappa}^{\max}$	e or \bar{e}	multi-layered
3D-Bead	0.487	0.072	
1D-Bead	0.421*	0.214*	
Radial-layer	0.386*	0.233*	✓
Spherical-layer	0.447	0.079	✓

*: The value is the average against twist angle γ .

A mark ✓ indicates that the unit has a multilayered structure.

$d/r = 1.2$ and $\kappa^{\max} = 0.447$ for the spherical-layer-type unit, the approximation error is 0.079.

For the one-DoF linkage model, the approximation error is numerically calculated. Similar to the calculation of the maximum curvature, we calculate the approximation error as a function of the twist angle γ [Fig. 10 right]. From this result, the approximation error ranges are $e \in [0.171, 0.225]$ for the 1d-bead-type unit and $e \in [0.186, 0.245]$ for the radial-layer-type unit. Furthermore, the average approximation error \bar{e} with respect to the twist angle γ is $\bar{e} = 0.214$ for the 1d-bead-type unit and $\bar{e} = 0.233$ for the radial-layer-type unit.

C. DISCUSSION AND CONCLUSION

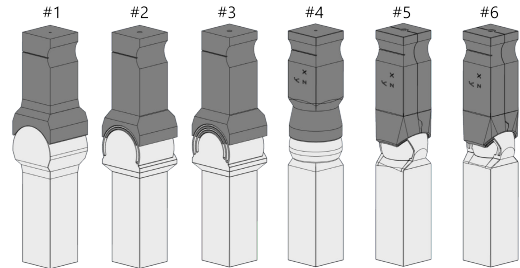
From the above, the maximum curvatures κ^{\max} and approximation errors e determined by the geometric properties of each unit are summarized in Table 2. The larger the curvature κ^{\max} and the smaller the error e , the higher the fitting performance of the string jamming mechanism. It was found that the spherical-layer-type unit, which is the proposed shape, has high fitting performance after the plain 3d-bead-type unit, which has best fitting performance. Moreover, the radial-layer-type unit, which is multilayered like the spherical-layer-type unit, has a maximum curvature κ^{\max} about 20% worse than that of the 3d-bead-type unit and an approximation error e about 220% worse. In contrast, the maximum curvature κ^{\max} and the approximation error e of the spherical-layer-type unit are only about 8% worse than those of the 3d-bead-type unit, and it can be said that the spherical-layer-type unit maintains high fitting performance even with the shape change due to multilayering.

V. EXPERIMENTS MEASURING THE HOLDING TORQUE

Another characteristic of the string jamming mechanism is the holding torque, which is the resistance force against external load. The holding torque is qualitatively better for multilayered units (comb-layer and spherical-layer) than for non-layered units (3d-bead and radial-layer). In fact, regarding the effect of cylindrical multilayering, the holding torque of the radial-layer-type unit is 1.3 – 3.3 times that of the 3d-bead-type unit, according to Mukaide et al. [10] and Michikawa et al. [14]. However, these studies only investigated the cylindrical plates' shape and did not clarify the effect of the number of layers. Moreover, the holding torque of multilayered units varies greatly with minute changes in the fabrication process, even if the material of each unit is the same. Thus, it is difficult to compare the numerical values with existing studies. Therefore, in this

TABLE 3. Test parts for the experiment that the holding torques are measured.

Part No.	Unit type	DoF	Layer
#1	1D-Bead	1	0
#2	Radial-layer with one layer	1	1
#3	Radial-layer with two layer	1	2
#4	3D-Bead	3	0
#5	Spherical-layer with one layer	3	1
#6	Spherical-layer with two layer	3	2



section, we clarify the effect of the proposed spherical shell structure and the existing cylindrical structure on the holding torque by fabricating prototypes and measuring the holding torque. We compare the holding torque of six types of units (#1 – 6) for two kinds of DoFs and three kinds of layers, as shown in Table 3.

A. METHOD

The experimental setup is shown in Figs. 11 (a) and (b). Test parts comprising a pair of units with both ends extended like rods were used in the measurement, and Fig. 11 (c) shows an example of the test parts #5. The dimensions of the units are the same as those in Section III-C. The cylinder height of the 1d-bead- and radial-layer-type units is arbitrary, but we set it to $2r = 13.5 \times 2 = 27$ mm to ensure a fair comparison with the 3d-bead- and spherical-layer-type units. The test parts were manufactured using an optical 3D printer, Form4 (Formlabs Inc.). All parts were made from the same material used in Section III-C, and the stacking direction was unified such that the longitudinal direction of the rods was set at a 5° angle to the stacking platform. Sufficient cleaning and secondary curing were performed to prevent the surface from becoming sticky. One side of the test parts was clamped, and a force gauge applied a vertical load F at a distance l from the center of rotation on the other side. For measurement around the x axis, an additional jig was attached to the loaded side to ensure a sufficient distance l [Fig. 11 (b)].

For each of the following conditions, the maximum applied external torque τ^{ex} at which the test part did not rotate was recorded as the holding torque τ . Measurements were taken for test parts #1 – 6 in Table 3. For test parts #1 – 3, the rotation directions were only around the z axis of the coordinate frame defined in Fig. 11 (c). For test parts #4 – 6, the rotation directions were around the x , y , and z axes of the coordinate frame defined in Fig. 11 (c). According to existing studies [10], [14], [16], the holding torque changes linearly in

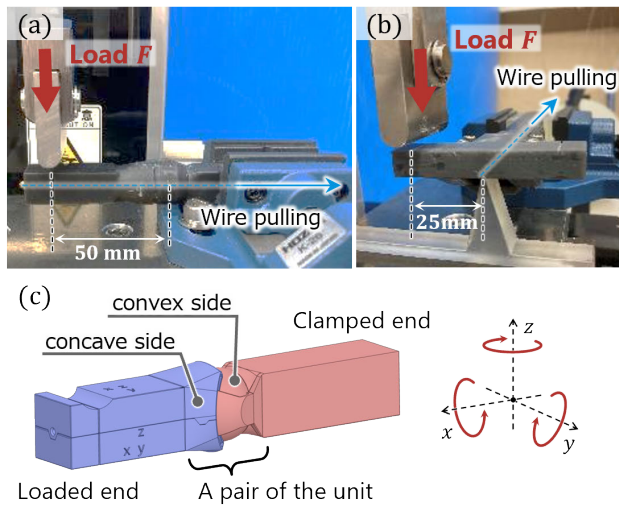


FIGURE 11. (a) Measurement around the y and z axes. (b) Measurement around the x axis. (c) Example of test parts #5.

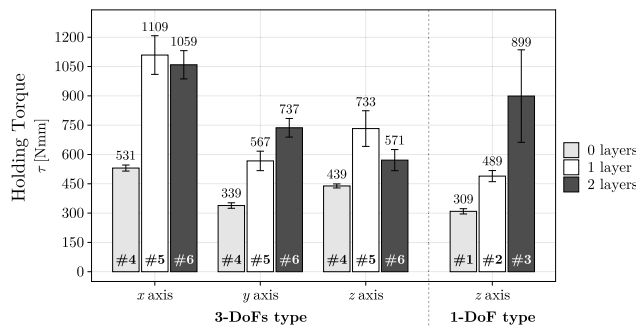


FIGURE 12. Measurements of the holding torque when the wire tension is 40 N.

the range of wire tension between 15 N and 80 N. Therefore, the wire tension was set to 40 N, as it falls within this range.

B. RESULTS

Figure 12 shows the measurement results. The vertical axis shows the holding torque, and the horizontal axis shows the conditions. The conditions on the horizontal axis are grouped and arranged based on the DoFs and the rotation directions of the load. The number of test parts used for each condition is shown in the bars of the graph. The holding torque τ is calculated as

$$\tau = \frac{1}{m} \sum_{k=1}^m l F^{\max,k}, \quad (11)$$

where the length of the beam is $l = 0.025$ m around the x axis and $l = 0.05$ m around the y and z axes, $F^{\max,k}$ is the local max load in the k -th trial for each experimental condition, and $m = 10$ is the number of valid trials. The Smirnov–Grubbs test was conducted recursively for the data set of each condition to determine outliers.

For all load directions, the multilayered units #2 and #3 (spherical-layer-type) and #5 and #6 (radial-layer-type) showed higher holding torque than the single-layered units #1 and #4, respectively [Fig. 12]. Thus, it was confirmed that

previous studies are reproduced and that the multilayering of the proposed spherical shell structure improves the holding torque. However, for the three-DoF units #5 and #6, contrary to expectations, there are cases where the holding torque does not improve even with an increase in the number of layers. We will discuss this result later.

C. DISCUSSION

Figure 12 shows that the cylindrical multilayer structure improves the holding torque by comparing units #1 and #2, #3. Similarly, multilayering the spherical shell structure improves the holding torque by comparing units #4 and #5, #6. Strictly predicting the holding torque is difficult because it is driven by frictional forces, but several existing studies [11], [14] have provided the following approximate formula for the theoretical holding torque τ_{th} :

$$\tau_{th} = \sum_i \mu T_i \hat{r}_i \quad (12)$$

where μ is the friction coefficient, T_i is the contact force generated from the wire tension, and \hat{r}_i is the radius of the i -th friction surface of the multilayer structure. The friction coefficient μ is assumed to be constant across the different layers. Existing studies assume that the contact force $T_1 = T_2 = \dots = T_i$ is constant. From this theoretical formula (12), it can be explained that the holding torque improves with the number of layers. However, a detailed examination reveals that the holding torque increases monotonically with the number of layers in the one-DoF type #1 – 3, but the increase in the number of layers does not always lead to an increase in the holding torque in the three-DoFs type #4 – 6. We will discuss this result later.

First, we compared the results of this study with the results of the existing studies that investigated the radial-layer-type unit [10], [14]. However, the friction coefficient can easily vary depending on the material and fabrication process of the unit, so it is difficult to compare the measured holding torque values with those of existing studies. In discussing the improvement in holding torque due to multilayering, it is appropriate to compare the improvement ratio based on the 3d-bead- and 1d-bead-types without multilayering. Table 4 shows the improvement ratio for each condition. The values for #1, 2, and 3 are calculated based on the 1d-bead-type unit #1. The values for #4, 5, and 6 are calculated based on the 3d-bead-type unit #4 for each axis.

The improvement ratio of the radial-layer-type unit with one layer was reported to be approximately 1.5 times by Michikawa et al. [14], and the result of this study was 1.58 times, which is close to that value [Table 4, #2]. Moreover, the improvement ratio of the radial-layer-type unit with two layers was reported to be approximately 1.3 times by Mukaide et al. [10], while the result of this study was 2.91 times, which is significantly higher [Table 4, #3]. Considering that the improvement ratio of the radial-layer-type unit with one layer reported so far is 1.5 times, it is questionable that the improvement ratio

TABLE 4. Improvement ratio of the holding torque against zero-layer units for each condition.

Part No.	DoF	Layer	Improvement ratio		
			x-axis	y-axis	z-axis
#1	1	0	—	—	1.00
#2	1	1	—	—	1.58
#3	1	2	—	—	2.91
#4	3	0	1.00	1.00	1.00
#5	3	1	2.09	1.67	1.67
#6	3	2	2.00	2.17	1.30

The one-DoF units #1, 2, 3 is compared with the unit #1.
The three-DoF units #4, 5, 6 is compared with the unit #4 for each axis.

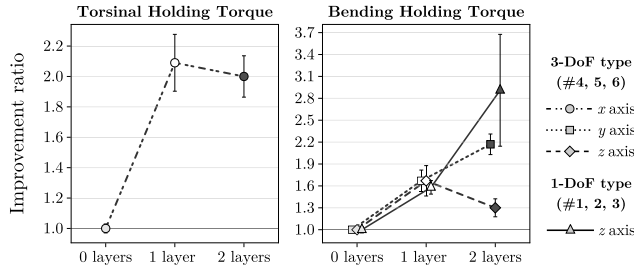


FIGURE 13. Improvement ratio of the holding torque τ compared to zero-layer units (#1 for the 1-DoF unit, #4 for the 3-DoF unit). The color indicates the number of layers, same as Fig. 12.

of the radial-layer-type unit with two layers is lower at 1.3 times. Existing studies have shown that various factors of the multilayer structure can cause the measured holding torque to fall below its potential value [14]. The strength of the multilayer structure may have been low in the study by Mukaide et al., and the holding torque could not be fully exerted. This insufficient strength is likely caused by the small unit radius and the fact that the two cylindrical plates occupy 53% out of a unit radius of 7.5 mm. In this study, the unit radius is larger (13.5 mm) and the cylindrical plates only occupy 30% out of a unit radius, thus the strength of the total structure has been improved. Therefore, it is considered that the potential holding torque of the two-layer unit could be fully realized by the improved strength.

Second, we compared the results with the three-DoF unit in our previous study [15]. In the previous study, the improvement ratios of the three-DoF unit with one layer were reported as 1.34 around the x axis, 1.20 around the y axis, and 1.13 around the z axis, relative to the 3d-bead-type unit. In comparison, the improvement ratios observed in this study were 2.09 for the x axis, 1.67 for the y axis, and 1.67 for the z axis, demonstrating a notable enhancement over the previous design. This improvement is attributed to an increase in the parameter β compared to the previous design [15], which likely enhanced the strength and friction of the multilayer structure.

Next, we compare the improvement ratio of the holding torque against the twisting moment [Fig. 13 left]. The conditions of the twisting holding torque correspond to the three-DoFs unit rotating around the x axis (○). Both the one-layer and two-layers have an improvement ratio of about 2, and although a relatively large improvement ratio was obtained, no further enhancement in the improvement ratio was observed with the increase in the number of layers.

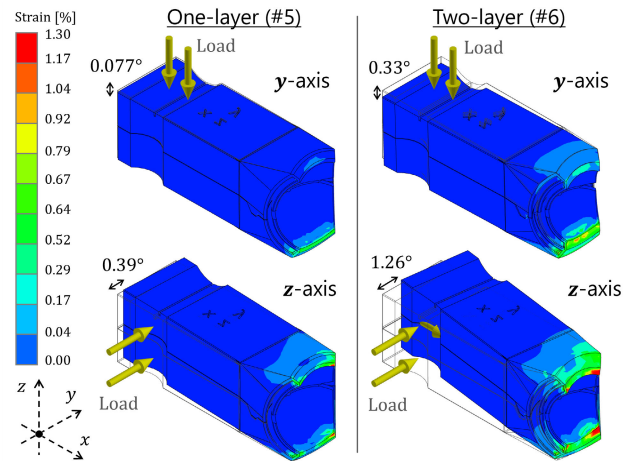


FIGURE 14. Example of FEM analysis results of the three-DoFs type test parts (#5, 6) under 10N loads. The color indicates the strain distribution. The load is applied in each direction at 50 mm point from the center of unit. The material is assumed to be isotropic ABS.

Finally, we compare the improvement ratio of the bending holding torque [Fig. 13 right]. The conditions of the bending holding torques correspond to the three conditions of the one-DoF units rotating around the z axis (△) and the three-DoFs units rotating around the y and z axes (□, ◇). In all three conditions (△, □, ◇), the improvement ratio of the one-layer is about 1.6, showing a common trend of improved holding torque due to multilayering. For the two-layer units, the one-DoF units rotating around the z axis (△) and the three-DoFs units rotating around the y axis (□) show a similar improvement ratio trend. However, the improvement ratio of the three-DoFs units rotating around the z axis (◇) is lower for the two-layer units than for the one-layer units.

The low improvement ratio is likely due to the low bending strength around the z axis of the multilayer structure. If a significantly low strength area exists in the test parts, the holding torque will be measured as low due to insufficient reaction force generation. The spherical shell plate of the multilayer structure must have a certain degree of flexibility to press the clearance caused by the wire tension, which inevitably reduces its strength. In particular, the concave plate is divided along the $y = 0$ section for assembly, further lowering its strength. We conducted FEM analysis of the test parts to compare the strength relative to the number of layers and to confirm the anisotropy in bending strength around the y and z axes. As an example of the results, we show the strain represented by color in Fig. 14. For visibility, the convex side of the test unit is omitted, and the concave side is used. It is found that the beam-like shape of the test parts have sufficient strength, but the edge of the concave plate of the multilayer structure is strained under all conditions, indicating low strength.

Figure 15 shows the graph of the change in the displacement angle for various loads in the FEM analysis. Here, the slope of the regression line can be regarded as the bending strength of the concave multilayer structure. From Fig. 15, it can be observed that the one-DoF units with one and two

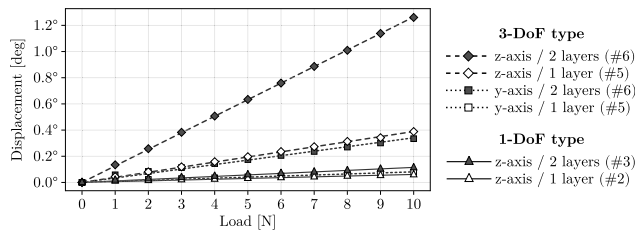


FIGURE 15. Displacement angles of the extended rods of the test parts in the FEM analysis.

layers (Δ , \blacktriangle) and the three-DoFs units with one layer around the y axis (\square) are the strongest. Moreover, in the three-DoF units, the one-layer unit around the z axis (\diamond) and the two-layer unit around the y axis (\blacksquare) exhibit similar strength. The two-layer unit around the z axis (\blacklozenge) is about three times weaker than the two-layer unit around the y axis (\blacksquare). This significant weakness likely explains the low improvement ratio in holding torque.

D. CONCLUSION

This experiment confirmed the effect of multilayering in the spherical-layer-type unit on improving the holding torque. However, unlike the radial-layer-type unit, the spherical-layer-type unit has certain rotation directions in which the holding torque does not increase, despite additional layers. The FEM analysis suggested that the multilayer structure of the spherical-layer-type unit significantly weakens the strength of the concave side as more layers are added, preventing the expected improvement. In contrast, the radial-layer-type unit with cylindrical plates shows a relatively low reduction in strength as the number of layers increases from one to two, resulting in a higher improvement ratio. The results indicate that the actual holding torque is affected by the positive effect of increased frictional force due to multilayering and the negative effect of decreased strength from the added structural complexity.

Enhancing the strength of the spherical-layer-type unit remains challenging, as simple shape improvement, such as increasing thickness, is difficult due to geometric constraints imposed by its range of motion. Furthermore, increasing overall rigidity prevents the layers with clearances from making proper contact, meaning the expected increase in frictional force from multilayering cannot be achieved. To enhance strength while maintaining both the range of motion and ease of compressing clearances, one potential solution is to combine the use of metal materials to improve base strength with shape optimization to selectively reduce rigidity. While simulating the holding torque itself is difficult, the selective reduction of rigidity can be verified through FEM analysis, providing a guideline for future design improvements.

VI. SUMMARY AND FUTURE WORKS

This study developed a spherical-layer-type unit for a string jamming mechanism that can transition between soft and

rigid states. The spherical-layer-type unit has achieved an enhancement of holding torque in the rigid state while maintaining good fitting performance in the soft state, compared to the 3d-bead-type unit. This unit's defining feature is its multilayer structure of spherical shell plates allowing three-DoFs motion and enhancing holding torque through increased frictional force. To achieve a spherical multilayer structure that does not allow bead-like connection through translational movement, we inherited the basic concept of assembly after divided molding [15] and redesigned the unit to enhance fitting performance and holding torque.

To consistently evaluate the fitting performance of the one-DoF and three-DoF units, we proposed two metrics: maximum curvature and approximation error relative to the minimum curvature circle. The string jamming mechanism composed of the spherical-layer-type unit showed an improvement of approximately 15% in maximum curvature compared to the radial-layer-type unit, which also has a multilayer structure. Furthermore, it reduced the approximation error to roughly one-third compared to the radial-layer-type unit.

Through holding torque measurement experiments, we examined the effects of the different multilayer structures of the radial-layer-type and spherical-layer-type units. In particular, unlike previous studies, we comprehensively verified the influence of the number of layers in the multilayer structure. The results showed that the holding torque of the radial-layer-type unit increased with the number of layers. Additionally, the spherical-layer-type unit generally improved holding torque through multilayering. However, holding torque showed minimal change with layer count for rotation around the x axis, increased with layers for rotation around the y axis, and decreased with layers for rotation around the z axis.

The measurement results of the holding torque improvement ratio indicate that the spherical-layer-type unit is not simply a superior version of the radial-layer-type unit. There is a trade-off between the spherical-layer-type unit's superior fitting performance from its high DoFs, and the radial-layer-type unit's higher holding torque due to its high-strength multilayer structure. Each unit can be utilized according to its specific characteristics, making them suitable for distinct applications. Regarding shape, the radial-layer-type unit can adjust both the height and the radius of the cylinder, whereas the spherical-layer-type unit can only adjust the radius. This difference in shape flexibility allows the radial-layer-type unit to accommodate a wider range of shapes. These characteristics are especially suitable for applications that differ from bead-like shapes, such as tactile feedback devices and the finger parts of two-finger grippers [14], [20]. In contrast, for constructing large, fabric-like variable stiffness structures using a string jamming mechanism, units with higher DoFs are considered more suitable [10]. Additionally, the spherical-layer-type unit, which balances bead-like shapes and the transmission of large forces, is more suitable for applications such as flexible manipulators [17].

In the future, the main challenge is to improve the strength of the spherical shell multilayer structure. The trade-off between the spherical-layer-type and radial-layer-type units is likely due to the low strength of the spherical shell structure. Simply increasing rigidity may decrease frictional force, so material improvement and shape optimization of the multilayer structure are necessary. Additionally, a detailed analysis of holding torque, including multilayer structure deformation, is needed. Moreover, for practical applications, it is necessary to consider improving holding torque through changes in material and manufacturing methods. Material considerations are also essential for improving long-term durability.

REFERENCES

- [1] M. E. Cates, J. P. Wittmer, J.-P. Bouchaud, and P. Claudin, "Jamming, force chains, and fragile matter," *Phys. Rev. Lett.*, vol. 81, no. 9, pp. 1841–1844, Aug. 1998.
- [2] J.-N. Roux, "Geometric origin of mechanical properties of granular materials," *Phys. Rev. E, Stat. Phys. Plasmas Fluids Relat. Interdiscip. Top.*, vol. 61, no. 6, pp. 6802–6836, Jun. 2000.
- [3] Y. Chen, J. H. Chang, A. S. Greenlee, K. C. Cheung, A. H. Slocum, and R. Gupta, "Multi-turn, tension-stiffening catheter navigation system," in *Proc. IEEE Int. Conf. Robot. Autom.*, May 2010, pp. 5570–5575.
- [4] E. Brown, N. Rodenberg, J. Amend, A. Mozeika, E. Steltz, M. R. Zakin, H. Lipson, and H. M. Jaeger, "Universal robotic gripper based on the jamming of granular material," *Proc. Nat. Acad. Sci. USA*, vol. 107, no. 44, pp. 18809–18814, Nov. 2010.
- [5] Y. Li, Y. Chen, Y. Yang, and Y. Wei, "Passive particle jamming and its stiffening of soft robotic grippers," *IEEE Trans. Robot.*, vol. 33, no. 2, pp. 446–455, Apr. 2017.
- [6] J. Choi, D.-Y. Lee, J.-H. Eo, Y.-J. Park, and K.-J. Cho, "Tendon-driven jamming mechanism for configurable variable stiffness," *Soft Robot.*, vol. 8, no. 1, pp. 109–118, Feb. 2021.
- [7] V. Wall, R. Deimel, and O. Brock, "Selective stiffening of soft actuators based on jamming," in *Proc. IEEE Int. Conf. Robot. Autom. (ICRA)*, May 2015, pp. 252–257.
- [8] I. Zubrycki and G. Granosik, "Novel haptic device using jamming principle for providing kinaesthetic feedback in glove-based control interface," *J. Intell. Robotic Syst.*, vol. 85, nos. 3–4, pp. 413–429, Mar. 2017.
- [9] T. Fujimoto, T. Shimizu, A. Nishimura, A. Nomura, H. Tetsui, M. Fujita, E. Takane, H. Komatsu, K. Tadakuma, M. Konyo, and S. Tadokoro, "Jamming transition line mechanisms with single dimension," in *Proc. Soc. Instrum. Control Eng. Tohoku Chapter 312-th Res. Meeting*, 2017, p. 5.
- [10] R. Mukaide, M. Watanabe, K. Tadakuma, Y. Ozawa, T. Takahashi, M. Konyo, and S. Tadokoro, "Radial-layer jamming mechanism for string configuration," *IEEE Robot. Autom. Lett.*, vol. 5, no. 4, pp. 5221–5228, Oct. 2020.
- [11] I. Onda, K. Tadakuma, M. Watanabe, K. Abe, T. Watanabe, M. Konyo, and S. Tadokoro, "Highly articulated tube mechanism with variable stiffness and shape restoration using a pneumatic actuator," *IEEE Robot. Autom. Lett.*, vol. 7, no. 2, pp. 3664–3671, Apr. 2022.
- [12] I. Onda, M. Watanabe, K. Tadakuma, K. Abe, and S. Tadokoro, "Tube mechanism with 3-axis rotary joints structure to achieve variable stiffness using positive pressure," *IEEE Robot. Autom. Lett.*, vol. 9, no. 1, pp. 675–682, Jan. 2024, doi: [10.1109/LRA.2023.3234767](https://doi.org/10.1109/LRA.2023.3234767).
- [13] K. Tadakuma, T. Fujimoto, M. Watanabe, T. Shimizu, E. Takane, M. Konyo, and S. Tadokoro, "Fire-resistant deformable soft gripper based on wire jamming mechanism," in *Proc. 3rd IEEE Int. Conf. Soft Robot. (RoboSoft)*, May 2020, pp. 740–747.
- [14] R. Michikawa, T. Endo, and F. Matsuno, "A multi-DoF exoskeleton haptic device for the grasping of a compliant object adapting to a user's motion using jamming transitions," *IEEE Trans. Robot.*, vol. 39, no. 1, pp. 373–385, Feb. 2023.
- [15] R. Michikawa, K. Tadakuma, and F. Matsuno, "A new design of multilayered string jamming mechanism with three-degree-of-freedom," in *Proc. IEEE/RSJ Int. Conf. Intell. Robots Syst. (IROS)*, Oct. 2023, pp. 8349–8355.
- [16] H. Miida, M. Watanabe, K. Tadakuma, K. Abe, I. Onda, and S. Tadokoro, "Dish-shaped thin beads: A novel bead shape for wire-driven variable stiffness mechanisms," in *Proc. IEEE 7th Int. Conf. Soft Robot. (RoboSoft)*, Apr. 2024, pp. 629–636.
- [17] I. Onda, M. Watanabe, K. Tadakuma, E. Takane, M. Konyo, and S. Tadokoro, "Pneumatic driven hollow variable stiffness mechanism aiming non-contact insertion of telescopic guide tubes," in *Proc. IEEE 4th Int. Conf. Soft Robot. (RoboSoft)*, Apr. 2021, pp. 615–621.
- [18] T. Takemori, M. Tanaka, and F. Matsuno, "Ladder climbing with a snake robot," in *Proc. IEEE/RSJ Int. Conf. Intell. Robots Syst. (IROS)*, Oct. 2018, pp. 1–9.
- [19] P. E. Black. (2004). *Hausdorff Distance*. [Online]. Available: <https://www.nist.gov/dads/HTML/hausdorffdst.html>
- [20] T. Takemori, M. Miyake, T. Hirai, X. Wang, Y. Fukao, M. Adachi, K. Yamaguchi, S. Tanishige, Y. Nomura, F. Matsuno, T. Fujimoto, A. Nomura, H. Tetsui, M. Watanabe, and K. Tadakuma, "Development of the multifunctional rescue robot FUHGA2 and evaluation at the world robot summit 2018," *Adv. Robot.*, vol. 34, no. 2, pp. 119–131, Jan. 2020, doi: [10.1080/01691864.2019.1697751](https://doi.org/10.1080/01691864.2019.1697751).



RYOHEI MICHIKAWA received the M.S. degree in engineering from the Graduate School of Engineering, Kyoto University, Kyoto, Japan, in March 2022, where he is currently pursuing the Ph.D. degree in mechanical engineering.

His research interests include haptic interfaces and the development of rescue robots.



FUMITOSHI MATSUNO (Senior Member, IEEE) received the Dr. (Eng.) degree from Osaka University, in 1986.

He is currently a Full Professor with Osaka Institute of Technology, a Professor Emeritus of Kyoto University, and the Deputy Director of Field of Robotics of Fukushima Institute of Research, Education and Innovation (F-REI). The F-REI is a special legal entity that was newly established by the Government of Japan, in April 2023. He is also the Vice-President of the NPO International Rescue System Institute and served as the President of the Institute of Systems, Control, and Information Engineers (ISCIE), and the Vice-President of the Robotics Society of Japan (RSJ). His research interests include bio-inspired robotics, modular robotics, rescue robotics, control of distributed parameter system and nonlinear systems, and swarm intelligence. He received numerous awards, including the Best Paper Awards, in 1986, from ISCIE, in 2001, 2006, and 2017, from the Society of Instrument and Control Engineers (SICE), in 2013, from the Information Processing Society of Japan, in 2018, from the RSJ, and the Prize for Academic Achievement from Japan Society of Mechanical Engineers (JSME), in 2009. He led his team, SHINOBI, to first place in RoboCup Rescue World competitions multiple times.

Dr. Matsuno served as the General Chair for IEEE SSR2011, IEEE/SICE SII2011, SWARM2015, DARS2021, and ASCC2022.

• • •